# Reductive dechlorination of hexachlorobutadiene by a Pd/Fe microparticle suspension in dissolved lactic acid polymers: degradation mechanism and kinetics

Romain Rodrigues, Stéphanie Betelu, Stéfan Colombano, Guillaume Masselot, Théodore Tzedakis, Ioannis Ignatiadis

**To cite this version:**

# Reductive Dechlorination of Hexachlorobutadiene by a Pd/Fe Microparticle Suspension in Dissolved Lactic Acid Polymers: Degradation Mechanism and Kinetics
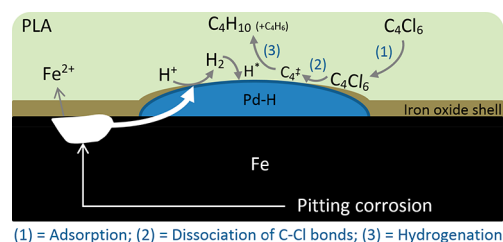
Romain Rodrigues,*,[†,‡,§] Stéphanie Betelu,[†] Stéfan Colombano,[†] Guillaume Masselot,[‡] Theodore Tzedakis,[§] and Ioannis Ignatiadis*,[†]

[†]BRGM (French Geological Survey), 3 avenue Claude Guillemin, 45060 Orléans Cedex 2, France

[‡]ADEME (French Environment and Energy Management Agency), 20 avenue du Grésillé, 49000 Angers Cedex 1, France

[§]LGC (Chemical Engineering Laboratory), 118 route de Narbonne, 31062 Toulouse Cedex 9, France

**ABSTRACT:** Reductive dechlorination of hexachlorobutadiene (HCBD) was performed by a suspension of scattered spots of palladium nanoparticles deposited on iron microparticles (nPd/$\mu$ZVI) in a mixture of dissolved lactic acid polymers and oligomers (referred to as PLA). The effects of nPd/$\mu$ZVI loading, temperature, HCBD initial concentration, and PLA content were investigated as to define the best conditions for the dechlorination. HCBD dechlorination by nPd/$\mu$ZVI occurred in a two-step process: first, HCBD adsorbed onto the nPd surface, which resulted in a rapid initial disappearance of pollutant in solution, and, second, it degraded chemically by atomic hydrogen



(1) = Adsorption; (2) = Dissociation of C-Cl bonds; (3) = Hydrogenation

H*, which resulted from the dissociative adsorption of $H_2$ on nPd. HCBD remained adsorbed on the surface until its complete degradation in nonchlorinated product, in agreement with the formation of an ordered activated complex on the nPd/$\mu$ZVI surface as suggested by the negative entropy of activation calculated from the Eyring equation. Hence, a minimum amount of nPd/$\mu$ZVI was required to enable simultaneously HCBD adsorption and $H_2$ production. In these cases, pseudo-first order rate equations were suitable to model HCBD disappearance kinetics. The increase in PLA content resulted in enhancing initial pH decrease such as to maintain acidic conditions and thus high reactivity over a longer period of time. It also resulted in enhancing the contact between HCBD and nPd/$\mu$ZVI, which was characterized by a more important initial adsorption. As a consequence, deviations from pseudo-first order kinetics were observed and a more representative model with a two-phase decay was proposed.

## 1. INTRODUCTION

Chlorinated organic compounds (COCs) are common dense nonaqueous phase liquid (DNAPL) contaminants of soil and groundwater. They represent a major concern for environment and human health due to the formation of large plumes of contamination and their slow natural attenuation.[1−3] Recovering contaminated sites is an important challenge in terms of sustainable development. Among all COC remediation technologies,[4−7] chemical reduction is one of the most important emerging techniques.

The use of zerovalent iron particles (ZVI) has been considered in the late 1970s[8] and was first applied for in situ remediation in the 1990s.[9,10] Particles have a core−shell structure with an iron core surrounded by a thin and defective mixed-valent iron oxide shell, in which remediation processes, such as adsorption and chemical reduction, occur.[11] The composition of the oxide shell is quite complex and can include—from the iron core to the oxide/water interface—Fe(II) oxide FeO, magnetite $Fe_3O_4$, maghemite $\gamma$-$Fe_2O_3$, hematite $\alpha$-$Fe_2O_3$, and goethite $\alpha$-FeOOH.[12−15] A good knowledge of the chemical properties and the structural evolution of this oxide shell is of crucial importance as they govern iron oxidation kinetics and degradation processes.[16]

In order to increase ZVI reactivity, especially on low molecular weight COCs for which low dechlorination rates were observed, many studies focused on the development of micro- and nanoscale bimetallic particles.[17] The use of a less active second metal allowed the formation of galvanic cells in which iron acts as anode and electrons donor, while the second metal acts as cathode and is protected from corrosion.[18,19] Several bimetallic combinations have been investigated, such as Pd/Fe, Ni/Fe, Cu/Fe, Ag/Fe, Au/Fe, and Pt/Fe.[17,20] Among all these metals, palladium (Pd) has shown the best improvement for COC dechlorination due to the adsorption of $H_2$ and its subsequent dissociation and accumulation in reactive atomic hydrogen H* on the metal.[21−23] Also, a lesser accumulation of reaction byproducts was reported[24,25] due to the total dissociation of C−Cl bonds on Pd surface.[26−28] The main degradation mechanism with Pd/Fe particles is therefore attributed to hydrodechlorination and hydrogenation reactions.

As limited mobility for micro- and nanoscale ZVI particles has been reported for in situ application,[29,30] different

polymers/polyelectrolytes—such as starch, gums, carboxymethyl cellulose and other biodegradable polymers—[20,31−41]are used in order to provide electrostatic forces to increase stability and to enhance transportability in porous sand media and in heterogeneous aquifer sediments.[42,43] The combined use of bimetallic particles and a stabilizer can therefore enhance conjointly stability, transportability, and reactivity of iron-based materials.[28,44,45]

The objectives of this study were to investigate the reductive dechlorination of hexachlorobutadiene (HCBD) by partially biologically produced nanosized palladium spots deposited on iron microparticles ($nPd/\mu ZVI$) in suspension in a mixture of dissolved lactic acid oligomers and polymers (simply referred as PLA in the manuscript). PLA is a biodegradable polyester which has been selected to increase the viscosity of the iron-based particle suspension to prevent aggregation and to provide hydrophobicity to the surface of the particles, in order to enhance the contact with the hydrophobic pollutant.[17] Also, the release of organic acids resulting from the hydrolysis of PLA is responsible for providing $H^+$ in the solution and at $nPd/\mu ZVI$-PLA interface, useful for promoting $nPd/\mu ZVI$ corrosion and minimizing the formation of a passive layer, such as iron hydroxides, iron oxy-hydroxides, and, if present, other precipitates (carbonates, nitrates, phosphates, or coprecipitation of heavy metals).[46] In the presence of a specific microbial community, lactic acid monomers can act as electron donors and hydrogen sources to stimulate an anaerobic reductive dechlorination.[47,48]

The effects of $nPd/\mu ZVI$ loading, temperature, HCBD initial concentration, and PLA content were investigated to provide better insight to HCBD reductive dechlorination. For each experiment, degradation was monitored by gas chromatography, for HCBD and its degradation byproducts contents, and by continuous temperature, pH, and redox potential measurements.

## 2. MATERIALS AND METHODS

**2.1. Materials.** HCBD (96%) was purchased from Sigma-Aldrich. Stock solutions of HCBD (5, 10, or 20 $g\cdot L^{-1}$) were prepared in methanol (HPLC grade, from VWR). Deionized water was obtained from a Milli-Q water system ($R = 18.2$ M$\Omega\cdot$cm) and degassed before any experiment by using first an ultrasonic bath (at 45 kHz) and $N_2$ flushing during the preparation of batch experiments.

The partially biologically produced palladium nanospots deposited on iron microparticles (BioCAT, noted as $nPd/\mu ZVI$) and the mixture of lactic acid polymers and oligomers (Dechlorem, noted as PLA) dissolved in ethyl lactate were provided by Biorem Engineering (Ghent, Belgium).[48] The particles were characterized before reaction by scanning electron microscopy coupled to energy dispersive X-ray (SEM/EDX) (Phenom XL, Fondis Bioritech, Voisins-le-Bretonneux, France) and BET-$N_2$ adsorption method (BELSORP-max, MicrotracBEL, Osaka, Japan). Briefly, the particles were spherical and in the size range of 1−20 $\mu m$ (Figure S1, see the Supporting Information), and the specific surface area was lower than 1 $m^2\cdot g^{-1}$.

The pH was measured with a glass electrode (pHG311-9, Hach Lange, Noisy Le Grand, France) calibrated before each experiment. Oxidation reduction potential (ORP) was measured with a platinum (Pt) electrode (XM150 Platinum Disc Electrode, Hach Lange, France). Both pH and ORP were measured with respect to a mercury-mercurous sulfate (MMS) reference electrode (Ametek SI, Elancourt, France), which is a chloride ion free reference electrode. All ORP are expressed in millivolts versus standard hydrogen electrode (mV/SHE).

**2.2. Batch Experiments.** Batch experiments were conducted in a 1 L cylindrical Pyrex double-walled water-jacketed reactor which is equipped with a mechanical propeller stirring rod (at 300 rpm) and with a reactor head with hermetic ports for setting up the electrodes, and for the introduction of the reactant and for the sampling. Measurements of pH, ORP, and temperature were continuously recorded with a data acquisition system (Keithley Instruments, model 2700, Cleveland, OH, USA) controlled via KickStart software.

A 1 mL portion of the appropriate stock solution was injected into the reactor filled with the degassed deionized water with initial zero-headspace conditions. Methanol represented only 0.1% of the total volume in order to minimize its inhibition effect on reduction by iron particles.[49] Reaction was initiated by the introduction of $nPd/\mu ZVI$ suspension in PLA, and 3 mL aliquots were collected at selected times. The reduction was stopped by the separation of the particles with powerful magnets. One mL of the supernatant aqueous phase without particles was collected and diluted (1:10) with degassed pure water into 20 mL headspace vials equipped with a PTFE septum. The prepared samples were finally stocked at 4 °C and analyzed within 24 h.

**2.3. Analytical Methods.** Samples were analyzed by GC using a Varian CP-3800 chromatograph controlled via Galaxie software and equipped with a DB-624 column (30 m × 0.32 i.d., with a 1.80 $\mu m$ film thickness) and a flame ionization detector (FID). Helium was chosen as carrier gas at 1.2 mL·min$^{-1}$ flow rate. Samples were heated at 80 °C for 30 min, and 200 $\mu L$ of the headspace gas was withdrawn by a gastight syringe and introduced in the injector chamber at 250 °C (1:25 split ratio). The oven was maintained at 35 °C for 5 min and, then, ramped to 245 °C at 10 °C·min$^{-1}$ with a hold for 10 min at this final temperature. The flame ionization detector (FID) temperature was maintained at 300 °C, with a He makeup at a flow rate of 30 mL·min$^{-1}$. Combustion in the FID was carried out with $H_2$ (30 mL·min$^{-1}$) and air (300 mL·min$^{-1}$). Seven reference standards of HCBD, ranging from 50 to 5000 $\mu g\cdot L^{-1}$, were periodically prepared and analyzed to ensure the proper quantification of the samples.

## 3. RESULTS AND DISCUSSION

**3.1. Reactivity of $nPd/\mu ZVI$ Suspension in PLA.** Due to the presence of $Fe^0$ core, nPd spots, and the iron oxide shell, the reactivity of $nPd/\mu ZVI$ involved different galvanic cells within the particles (Figure 1). The first current flowed from $Fe^0$ to nPd, the second from $Fe^0$ to the oxide shell,[50,51] and the third from the oxide shell to nPd. The first two currents were responsible for the enhancement of ZVI pitting corrosion. Hence, the $Fe^0$ core acted only as an anode and oxidized in $Fe^{2+}$. The third current was responsible for the anodic dissolution of the shell that encapsulated nPd spots.

Among these three currents, the one which flowed from $Fe^0$ to nPd was the more important as palladium is more noble than iron ($E°_{(Pd^{2+}/Pd)}$ = 0.915 V/SHE; $E°_{(PdOH^+,H^+/Pd)}$ = 0.983 V/SHE). Hence, nPd spots acted as the preferential cathode in this system for $H^+$ reduction.[52,53] Also, they allowed the dissociative absorption of $H_2$ in atomic hydrogen H*, with the accumulation of H-species into the metal.[21−23] The main mechanism for HCBD degradation was therefore attributed to hydrodechlorination and hydrogenation pathways.

**3.2. Effect of $nPd/\mu ZVI$ Loading.** The effect of $nPd/\mu ZVI$ loading was investigated with 150, 375, and 600 mg of $nPd/\mu ZVI$ at 25 °C, with 850 mg of PLA and 38.5 $\mu$M of HCBD. Results are shown in Figure 2. Initial amounts of 150 and 375 mg were not enough to obtain a complete degradation of 10 mg·L$^{-1}$ of HCBD
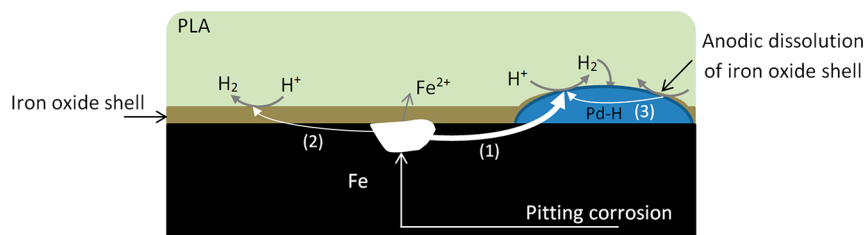
**Figure 1.** Schematic representation of the different corrosion currents which flow within nPd/μZVI. (1) Main current which flows from Fe⁰ to nPd. (2) Current which flows from Fe⁰ to the oxide shell. (3) Current which flows from the oxide shell to nPd.
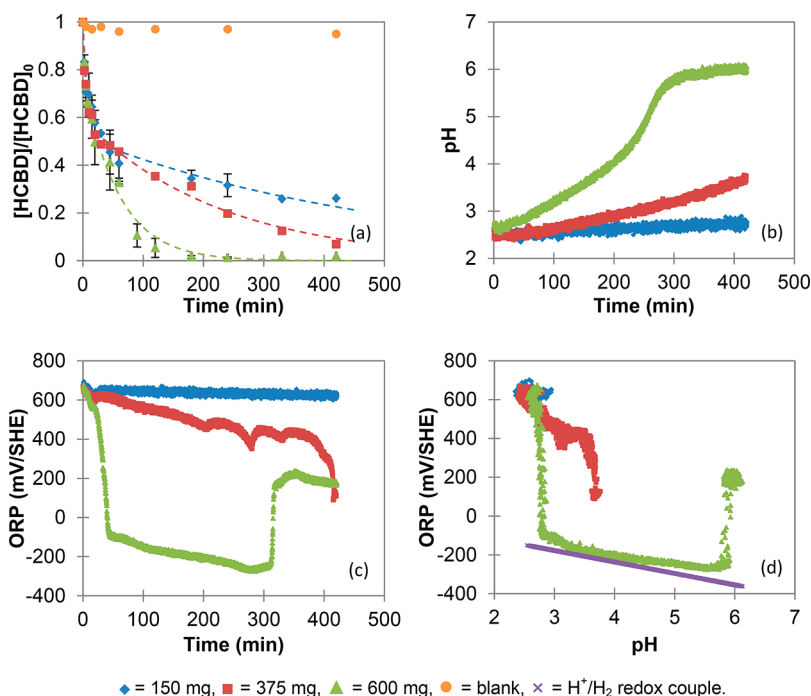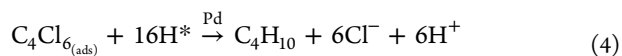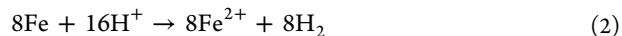


**Figure 2.** Effect of nPd/μZVI loading on HCBD dechlorination in Milli-Q water. (a) Evolution of HCBD concentration versus time. (b) Evolution of pH versus time. (c) Evolution of ORP versus time. (d) Evolution of ORP versus pH in 420 min. Experimental conditions: $[HCBD]_0 = 38.5\ \mu M$, $m_{PLA} = 850$ mg, $T = 25$ °C. Error bars in part a represent standard deviation for $n = 2$. Dashed lines represent the nonlinear regression of the adsorption/reduction model.

in 420 min; whereas, a complete degradation was observed in approximately 180 min with 600 mg (Figure 2a), with the production of butane as the main final product.

Two competitive phenomena occurred on the nPd/μZVI surface: H₂ production and HCBD adsorption. Concerning the first phenomenon, nPd acted as the preferential cathodic site for H⁺ reduction. Concerning the second one, HCBD adsorption could have been carried out on the entire surface of nPd/μZVI. However, as the amount of iron loaded in the reactor was though greater than the theoretical stoichiometric requirement of iron for HCBD reduction in butane in all cases (1.7 mg of iron per mg of HCBD) and the specific surface area was quite high, most adsorption of HCBD seemed to occur on nPd. As a result, H₂ production was less important when the amount of nPd/μZVI decreased, which can explain the slow disappearance of HCBD after 30 min of reaction with 150 and 375 mg. With 600 mg, active sites for both HCBD adsorption and H₂ production were always simultaneously available, thus enabling the complete dechlorination. Iron corrosion was thus cathodically controlled by the availability of nPd spots for H⁺ reduction. HCBD initial disappearance was attributed to its adsorption on nPd/μZVI and further disappearance to its reductive dechlorination by atomic hydrogen. This two-step process was consistent with the low

production of nonchlorinated product in the first minutes, and the more rapid and important accumulation of C₄ compounds when nPd/μZVI loading increased (Figure S2). The non-accumulation of reaction intermediates in water could indicate a rapid dechlorination due to the dissociation of C−Cl bond on the catalyst, followed by a progressive hydrogenation until the formation of nonchlorinated product. The proposed mechanism for HCBD dechlorination can be written with eqs 1−4:

$$C_4Cl_6 \rightarrow C_4Cl_{6(ads)} \tag{1}$$

$$8Fe + 16H^+ \rightarrow 8Fe^{2+} + 8H_2 \tag{2}$$

$$8H_2 \xrightarrow{Pd} 16H^* \tag{3}$$

$$C_4Cl_{6(ads)} + 16H^* \xrightarrow{Pd} C_4H_{10} + 6Cl^- + 6H^+ \tag{4}$$

As shown in Figures 2b and c, the introduction of the suspension fixed the initial pH to 2.75 and the initial ORP to 650 mV/SHE. This high positive ORP value was attributed to dominant Fe(III)/Fe(II) redox couples resulting from the partial dissolution at low pH of the iron oxide shell which covered the surface of the particles[54,55] and from the current which flowed from the oxide

shell to nPd (anodic dissolution of the shell that encapsulated nPd).

The temporal evolution of pH was related to the initial amount of nPd/$\mu$ZVI; the greater the amount of nPd/$\mu$ZVI, the faster the pH increased with time (Figure 2b). No accumulation of $H_2$ was observed on Pt electrode with 150 mg of nPd/$\mu$ZVI (Figure 2c), in agreement with a small production of $H_2$ and its consumption for HCBD dechlorination. With 375 mg, a slow decrease in ORP with time was observed for more than 200 min, followed by a rapid decrease in the last minutes of the reaction (Figure 2c). In the first minutes, degradation was limited by $H_2$ production as no accumulation was observed, and the slow decrease in ORP with time was attributed to an increase in $Fe^{2+}$ content, according to the Nernst eq (eq 5).

$$E_{Fe(III)/Fe(II)} = E^{\circ}_{Fe(III)/Fe(II)} + \frac{RT}{F}\ln\left(\frac{a_{Fe(III)}}{a_{Fe(II)}}\right) \tag{5}$$

where $E_{Fe(III)/Fe(II)}$ is the standard electrode potential, $R$ is the universal gas constant ($8.314$ J·mol$^{-1}$·K$^{-1}$), $T$ is the absolute temperature (K), $F$ is the Faraday constant ($96,485$ C·mol$^{-1}$), and $a_{Fe(III)}$ and $a_{Fe(II)}$ are the activities of Fe(III) and Fe(II), respectively.

Thereafter, as HCBD dechlorination occurred progressively, some active sites on nPd/$\mu$ZVI surface were again available for $H_2$ production due to butane desorption. Consequently, the change in redox couple was observed when HCBD concentration decreased and $H_2$ production increased, and the dominant redox couple became $H^+/H_2$ (Figure 2d, as a Pourbaix-type diagram). The increase in pH and the decrease in ORP are characteristics of iron oxidation and have already been observed.[56]

With 600 mg, a sufficient number of nPd/$\mu$ZVI sites were available for both reactions to observe a rapid change in redox couple (Figure 2c). A second change in redox couple was observed when the change in pH became slower. This last change was attributed to the decrease in $H^+$ content but also to the openings of the reactor for the sampling, which resulted in the evacuation of $H_2$ and the introduction of $O_2$. Hence, $Fe^{2+}$ produced during iron corrosion was progressively oxidized in nonsoluble Fe(III) species at these pH values. The particles were therefore progressively covered by a passivation layer. This change in chemical composition and structural properties of the shell caused a decrease in porosity and conductivity of the shell,[14,57] resulting in a decrease in iron oxidation rate and, thus, in $H_2$ production. The ORP value was then fixed by Fe(III)/Fe(II) redox couple species (Figure 2d).

A pseudo-first-order equation was used to describe HCBD degradation (eq 6):

$$-\frac{dC}{dt} = k_{obs}C \tag{6}$$

where $C$ is the concentration in HCBD (M) at time $t$ (min) and $k_{obs}$ is the pseudo-first-order rate constant (min$^{-1}$). Only the result with 600 mg of nPd/$\mu$ZVI is presented in Table 1, when the complete degradation was observed.

**3.3. Effect of Temperature.** Analysis of the effect of temperature was performed at 12, 25, and 35 °C with 600 mg of nPd/$\mu$ZVI, 850 mg of PLA, and 38.5 $\mu$M of HCBD (Figure 3). Results have shown that HCBD degradation was incomplete at 12 °C after 420 min, whereas the dechlorination was complete in about 90 min at 35 °C (Figure 3a). This is in agreement with the more rapid formation of $C_4$ compounds when the temperature increased (Figure S3).

**Table 1. Pseudo-first-order Rate Constants for HCBD Degradation in Milli-Q Water with 600 mg of Pd/Fe Microparticles**

| $m_{Pd/Fe}$ (mg) | $m_{PLA}$ (mg) | $T$ (°C) | [HCBD]$_0$ ($\mu$M) | $k_{obs}$ (min$^{-1}$) |
|---|---|---|---|---|
| 600 | 850 | 25 | 38.5 | 0.0235 ($R^2$ = 0.9798) |
| 600 | 1700 | 25 | 38.5 | 0.0189 ($R^2$ = 0.9621) |
| 600 | 3400 | 25 | 38.5 | 0.0176 ($R^2$ = 0.9177) |
| 600 | 850 | 12 | 38.5 | 0.0076 ($R^2$ = 0.9358) |
| 600 | 850 | 35 | 38.5 | 0.0324 ($R^2$ = 0.9605) |
| 600 | 850 | 25 | 17.0 | 0.0308 ($R^2$ = 0.9630) |
| 600 | 850 | 25 | 75.6 | 0.0232 ($R^2$ = 0.9911) |

An increase in temperature accelerated all the processes involved in corrosion.[58] Also, initial pH was lower at 35 °C than at 12 °C (Figure 3b). The increase in temperature led to an increase in the hydrolysis rate of PLA as this reaction—involving bond breaking—is endothermic (Le Chatelier's principle). A small decrease in temperature was also observed after the introduction of the reactant. Evolution of pH values clearly showed that corrosion was greater and faster at 35 °C than at 12 °C (Figure 3b). Thus, $H_2$ production was faster when the temperature was increased, which can explain the increase of dechlorination rate. ORP progressive fixation by $H^+/H_2$ redox couple occurred later when the temperature was increased from 25 to 35 °C (Figures 3c and d). Even if lower absorption efficiency of $H_2$ into palladium by increasing the temperature has been reported,[59,60] this later fixation was attributed to a more important dissolution of the iron oxide shell at low pH, resulting in higher initial content in Fe(III)/Fe(II) species.

Pseudo-first order equations were used to model the degradation in the first 120 min, and results are presented in Table 1. The Arrhenius equation was used to establish the relation between the rate constant and the temperature (eq 7).

$$\ln k_{obs} = \ln A - \frac{E_a}{RT} \tag{7}$$

where $k_{obs}$ is the constant rate (min$^{-1}$), $A$ is the pre-exponential factor (min$^{-1}$), $E_a$ is the activation energy (J·mol$^{-1}$), $R$ is the universal gas constant, and $T$ is the absolute temperature (K). An almost equivalent relationship, the Eyring equation, can be used by following the transition state theory (eq 8).

$$k_{obs} = \frac{k_B T}{h}\exp\left(\frac{-\Delta^{\ddagger}G^{\circ}}{RT}\right) \tag{8}$$

where $k_B$ is the Boltzmann constant ($1.381 \times 10^{-23}$ J·K$^{-1}$), $h$ is the Planck constant ($6.626 \times 10^{-34}$ J·s), and $\Delta^{\ddagger}G^{\circ}$ is the Gibbs energy of activation (J·mol$^{-1}$). The relation can also be written and linearized as (eq 9):

$$\ln\left(\frac{k_{obs}}{T}\right) = \frac{-\Delta^{\ddagger}H^{\circ}}{R}\frac{1}{T} + \ln\left(\frac{k_B}{h}\right) + \frac{\Delta^{\ddagger}S^{\circ}}{R} \tag{9}$$

where $\Delta^{\ddagger}H^{\circ}$ is the standard enthalpy of activation (J·mol$^{-1}$) and $\Delta^{\ddagger}S^{\circ}$ is the standard entropy of activation (J·mol$^{-1}$·K$^{-1}$). Results obtained from Arrhenius plots are $E_a = 47.1$ kJ·mol$^{-1}$ and $A = 3.42 \times 10^6$ min$^{-1}$ ($R^2$ = 0.955). As activation energies for mass transfer are generally reported in the range 15−30 kJ·mol$^{-1}$,[61] HCBD dechlorination is a reaction-limited process. Results obtained from the Eyring plot are $\Delta^{\ddagger}H^{\circ} = 44.6$ kJ·mol$^{-1}$ and $\Delta^{\ddagger}S^{\circ} = -162$ J·mol$^{-1}$·K$^{-1}$ ($R^2$ = 0.950). The negative value for the entropy of activation for HCBD reduction indicated a
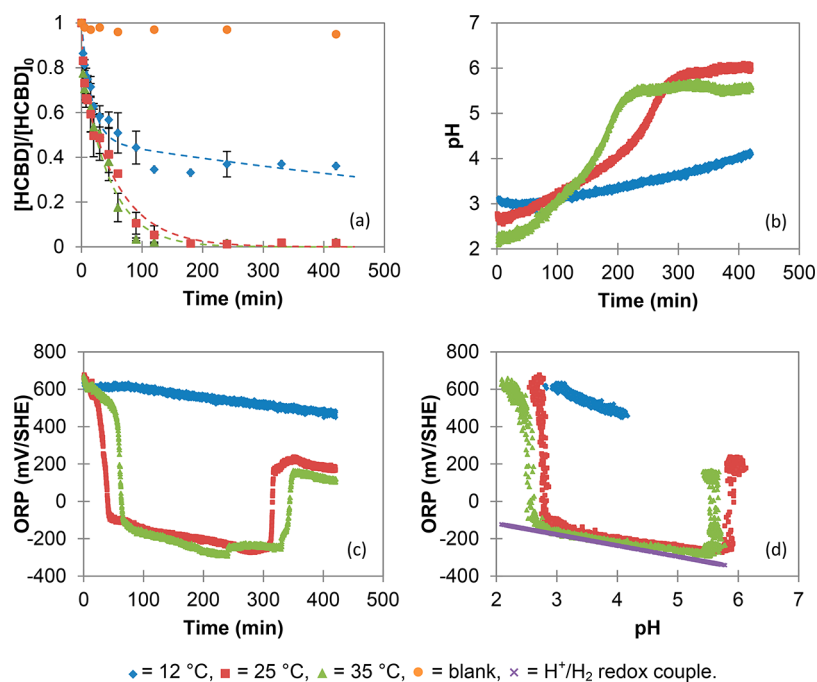
**Figure 3.** Effect of temperature on HCBD dechlorination in Milli-Q water. (a) Evolution of HCBD concentration versus time. (b) Evolution of pH versus time. (c) Evolution of ORP versus time. (d) Evolution of ORP versus pH in 420 min. Experimental conditions: $[HCBD]_0 = 38.5\ \mu M$, $m_{nPd/\mu ZVI} = 600$ mg, $m_{PLA} = 850$ mg. Error bars in part a represent standard deviation for $n = 2$. Dashed lines represent the nonlinear regression of the adsorption/reduction model.

decrease in degrees of freedom with the formation of an ordered activated complex,[62] characterized by the strong adsorption of HCBD on nPd/$\mu$ZVI until its complete dechlorination. Equation 4, previously proposed, can be written with eqs 10 and 11, involving an activated intermediate noted $C_4^{\ddagger}$.

$$C_4Cl_6 \xrightarrow{\text{Pd}} C_4^{\ddagger} + 6Cl^- \tag{10}$$

$$C_4^{\ddagger} + 16H^* \xrightarrow{\text{Pd}} C_4H_{10} + 6H^+ \tag{11}$$

**3.4. Effect of HCBD Initial Concentration.** The effect of initial concentration was performed with three initial concentrations —17.0, 38.5, and 75.6 $\mu$M—at 25 °C, with 600 mg of nPd/$\mu$ZVI and 850 mg of PLA. Results are presented in Figure 4. First, the change in initial concentration in these ranges did not have any influence on degradation pathways, with the production of nonchlorinated $C_4$ compounds as the final products (Figure S4). Pseudo-first-order rate constants (Table 1) decreased as the initial concentration increased. However, little variability in degradation rates were observed compared to the effect of nPd/$\mu$ZVI loading or temperature, which may indicate that in this concentration range the global reaction was controlled by the surface-reaction kinetic.[63] For the highest initial concentration, formation of iron (oxy-)hydroxides, resulting from the introduction of $O_2$ during the sampling, were observed and characterized by the decrease of pH values after 300 min of reaction (Figure 4b). As a consequence, ORP value increased as the pH decreased (Figures 4c and d).

**3.5. Effect of PLA Content.** The effect of PLA content was investigated with three initial contents —850, 1700, and 3400 mg—at 25 °C, with 600 mg of nPd/$\mu$ZVI and 38.5 $\mu$M of HCBD. Results are presented in Figure 5. The increase in PLA content increased HCBD disappearance in the first minutes (Figure 5a). As shown in Figure 5b, the pH remained stable only for a few minutes with 850 mg of PLA and for about 40 min with

3400 mg. The initial disappearance was therefore attributed to a more important adsorption on nPd/$\mu$ZVI surface. Indeed, PLA increased the hydrophobicity of the surface of the particles in order to promote the contact with HCBD. As a consequence, $H_2$ production was slower due to a decrease of available sites for $H^+$ reduction. As shown in Figure 5c, the change in redox couple occurred later when PLA content was increased. This phenomenon can be attributed to the slower initial production of $H_2$ and, as the effect of temperature, to the increase of iron oxide dissolution as the initial pH was lower, resulting in higher concentration of Fe(II) and Fe(III) species in solution that fixed the initial ORP values.

The decrease of initial pH was of great interest as acidic conditions were maintained over a longer period of time to prevent the formation of passivation layer and to preserve high reactivity of the iron-based particles.[63] As shown in Figures 5c and d with 1700 and 3400 mg of PLA, the dominant redox couple that controlled ORP value of the medium was $H^+/H_2$, even after 420 min.

As to confirm that reactivity was still important after 420 min, additional 38.5 $\mu$M of HCBD were respiked for experiments with 850 and 3400 mg of PLA, without the new addition of reactant (Figure 6). In both cases, HCBD dechlorination was more rapid for the second injection (after 3 h) as compared to the first injection, which can be explained by the initial presence of atomic hydrogen in the system. For the third injection after 6 h, degradation was very similar to that of the second injection with 3400 mg of PLA, whereas it was not complete with 850 mg. The increase in PLA content with the same amount of nPd/$\mu$ZVI was favorable to maintain high reductive conditions in the system. After 23 h, the degradation was still complete with 3400 mg of PLA, although a slower rate of disappearance was observed. This decrease in reactivity over time in both cases was attributed to the progressive encapsulation of nPd spots by an iron (oxy-)hydroxide shell,[64,65] especially with 850 mg of PLA.

Evolutions of pH and ORP with time are shown in Figures 6c and d. In both cases, the opening of the reactor for sampling led
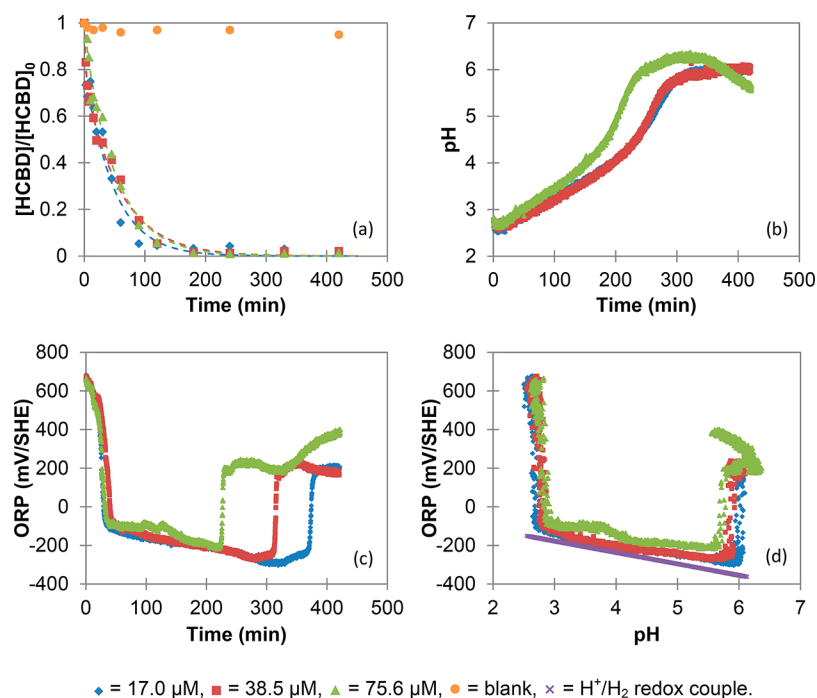
**Figure 4.** Effect of HCBD initial concentration on its dechlorination in Milli-Q water. (a) Evolution of HCBD concentration versus time. (b) Evolution of pH versus time. (c) Evolution of ORP versus time. (d) Evolution of ORP versus pH in 420 min. Experimental conditions: $m_{nPd/\mu ZVI}$ = 600 mg, $m_{PLA}$ = 850 mg, $T$ = 25 °C. Error bars in part a represent standard deviation for $n$ = 2. Dashed lines represent the nonlinear regression of the adsorption/reduction model.



**Figure 5.** Effect of PLA content on HCBD dechlorination in Milli-Q water. (a) Evolution of HCBD concentration versus time. (b) Evolution of pH versus time. (c) Evolution of ORP versus time. (d) Evolution of ORP versus pH in 420 min. Experimental conditions: $[HCBD]_0$ = 38.5 $\mu$M, $m_{nPd/\mu ZVI}$ = 600 mg, $T$ = 25 °C. Error bars in part a represent standard deviation for $n$ = 2. Dashed lines represent the nonlinear regression of the adsorption/reduction model.
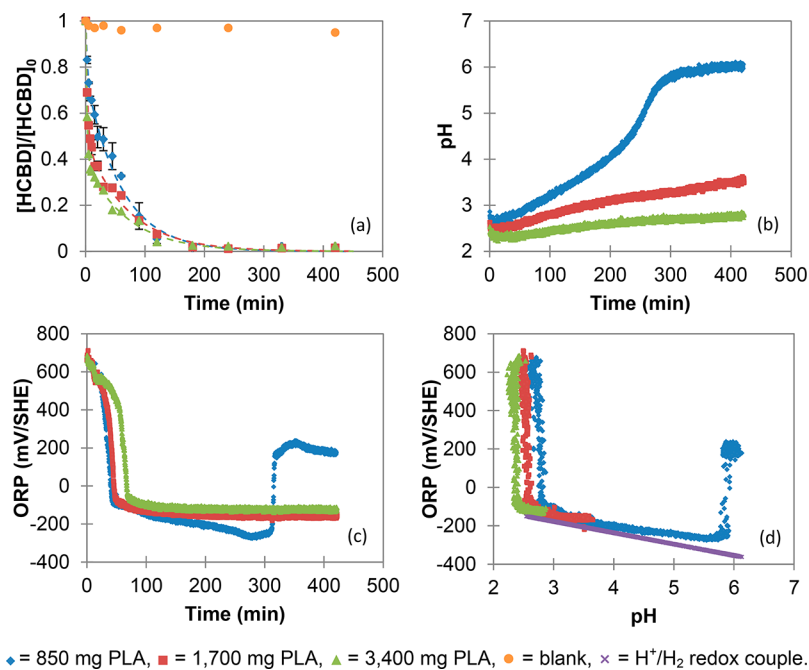
to the exhaust of $H_2$ and the introduction of $O_2$. With 850 mg of PLA, as the pH rapidly increased to 6, formation of nonsoluble iron species occurred rapidly and ORP was fixed by Fe(III)/Fe(II) redox species from 250 min (Figure 6c). However, with 3400 mg of PLA, ORP values became again progressively fixed by $H^+/H_2$ redox couple, even after the last sample at 1800 min

(Figure 6d), which confirmed that $H_2$ production was still important for the maintenance of highly reductive conditions.

**3.6. Modeling of Reaction Kinetics.** Pseudo-first-order rate equations fitted well with most experiments, as shown by the correlation coefficients ($R^2 > 0.9$) in Table 1. However, the initial disappearance, attributed to HCBD adsorption, was not
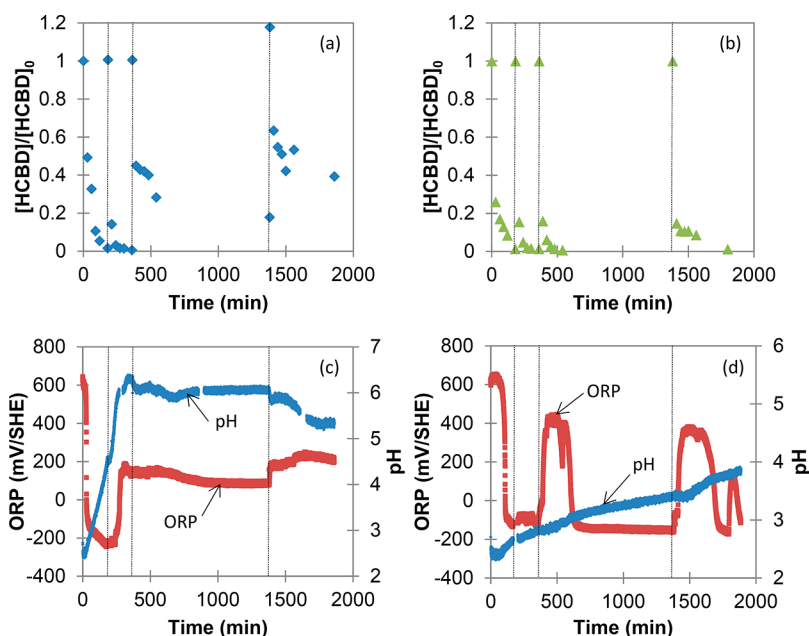
**Figure 6.** Effect of PLA content with successive injections of 38.5 $\mu$M of HCBD in the batch reactor. (a) Evolution of HCBD concentration versus time in the presence of 850 mg of PLA. (b) Evolution of HCBD concentration versus time in the presence of 3400 mg of PLA. (c) Evolution of pH and ORP versus time in the presence of 850 mg of PLA. (d) Evolution of pH and ORP versus time in the presence of 3400 mg of PLA. Experimental conditions: $[\mathrm{HCBD}]_0 = 38.5\ \mu$M, $m_{\mathrm{nPd}/\mu\mathrm{ZVI}} = 600$ mg, $T = 25\ °$C. Vertical lines indicate HCBD reinjection.

**Table 2. Fitted Data for HCBD Degradation Using a Nonlinear Least Squares Regression on the Adsorption/Reduction Model (Equation 12)**

| conditions | $\alpha$ | $k_a$ (min$^{-1}$) | $k_c$ (min$^{-1}$) | $R^2$ |
|---|---|---|---|---|
| 150 mg nPd/$\mu$ZVI | $0.484 \pm 0.033$ | $0.114 \pm 0.020$ | 0.002 | 0.973 |
| 375 mg nPd/$\mu$ZVI | $0.408 \pm 0.018$ | $0.206 \pm 0.030$ | 0.004 | 0.992 |
| 600 mg nPd/$\mu$ZVI | $0.237 \pm 0.037$ | $0.390 \pm 0.178$ | $0.017 \pm 0.002$ | 0.991 |
| 12 °C | $0.477 \pm 0.042$ | 0.001 | $0.059 \pm 0.011$ | 0.958 |
| 25 °C | $0.237 \pm 0.037$ | $0.387 \pm 0.176$ | $0.017 \pm 0.002$ | 0.990 |
| 35 °C | | | | |
| 17.0 $\mu$M | $0.163 \pm 0.035$ | | $0.022 \pm 0.002$ | 0.978 |
| 38.5 $\mu$M | $0.237 \pm 0.037$ | $0.387 \pm 0.176$ | $0.017 \pm 0.002$ | 0.990 |
| 75.6 $\mu$M | $0.057 \pm 0.124$ | $0.158 \pm 0.485$ | $0.019 \pm 0.003$ | 0.986 |
| 850 mg PLA | $0.237 \pm 0.037$ | $0.391 \pm 0.179$ | $0.017 \pm 0.002$ | 0.990 |
| 1700 mg PLA | $0.478 \pm 0.020$ | $0.014 \pm 0.001$ | $0.320 \pm 0.034$ | 0.996 |
| 3400 mg PLA | $0.388 \pm 0.014$ | $0.014 \pm 0.001$ | $0.443 \pm 0.037$ | 0.997 |

considered for this calculation. Furthermore, some deviations to pseudo-first-order were observed when the dechlorination was not complete (with 150 and 375 mg of nPd/$\mu$ZVI at 25 °C or with 600 mg of nPd/$\mu$ZVI at 12 °C). As a consequence, this model was inappropriate for a global representation of the reaction. In order to consider the importance of adsorption in these experiments, a new model was proposed (eq 12), derived from the one proposed by Wang et al.[66]

$$\frac{C}{C_0} = \alpha\exp(-k_a t) + (1 - \alpha)\exp(-k_c t) \tag{12}$$

where $C_0$ is the initial concentration of pollutant, $C$ is the pollutant concentration at time $t$ (min), $k_a$ and $k_c$ are respectively the rate constants for adsorption and chemical degradation, $\alpha$ represents the weight value for adsorption, and $1 - \alpha$ represents the weight value for chemical degradation. Results of nonlinear least-squares regressions of eq 12 are presented in Table 2. The high correlation coefficients ($R^2 > 0.95$) have shown that this model was representative of HCBD degradation by nPd/$\mu$ZVI suspension in PLA, especially when $\alpha > 0.35$. In the other cases, standard errors on one parameter or more were important, which

could indicate that the separation between adsorption and reduction was not relevant and the use of pseudo-first order equations was more suitable for the calculation of rate constants.

## 4. CONCLUSION

Reductive dechlorination of HCBD by nPd/$\mu$ZVI suspension in PLA solutions was investigated in batch experiments. The overall results have indicated that the dechlorination occurred in two steps: the adsorption of HCBD, mainly on nPd spots surface, and its chemical reduction by atomic hydrogen resulting from the dissociative adsorption of H$_2$ in Pd. Hence, a minimum amount of nPd/$\mu$ZVI was required to provide simultaneously a sufficient number of sites for HCBD adsorption and for H$_2$ production.

HCBD degradation led to the formation of butane as the main final product, without any accumulation of chlorinated by-products in solution, in agreement with the formation of an ordered activated complex on nPd/$\mu$ZVI surface proposed by the negative entropy of activation calculated from Eyring equation. Concerning the effect of nPd/$\mu$ZVI loading, temperature, and

HCBD initial concentration, pseudo-first-order rate equations were suitable to explain HCBD dechlorination.

The increase of PLA dosage was of great interest as acidic conditions were maintained over a longer period of time to prevent the formation of passivation layer and to preserve high reactivity of the iron-based particles, as indicated by the negative ORP values. Moreover, as PLA can promote contact between HCBD and nPd/$\mu$ZVI, a more important adsorption was observed. As a consequence, a two-phase decay model was proposed and used to consider that the two steps occurred consecutively. This model appeared to be very representative of HCBD dechlorination when the weight associated with both steps was important ($\alpha > 0.35$).

## ■ ASSOCIATED CONTENT

### ⓢ Supporting Information

The Supporting Information is available free of charge on the ACS Publications website at DOI: 10.1021/acs.iecr.7b03012.

SEM/EDX images of nPd/$\mu$ZVI (Figure S1) and the production of nonchlorinated $C_4$ compounds versus time for the effects of nPd/$\mu$ZVI loading, temperature, HCBD initial concentration, and PLA content (Figures S2–S5) (PDF)

## ■ AUTHOR INFORMATION

**Corresponding Authors**

*Mailing address: BRGM, 3 avenue Claude Guillemin, 45060 Orléans Cedex 2, France. Tel.: +33 2 38 64 35 10. E-mail address: r.rodrigues@brgm.fr (R.R.).

*Tel.: +33 2 38 64 35 59. E-mail address: i.ignatiadis@brgm.fr (I.I.).

**ORCID** ⓘ

Romain Rodrigues: 0000-0001-7302-4255

**Notes**

The authors declare no competing financial interest.

## ■ REFERENCES

(1) Stupp, H. D.; Paus, L. Migrationsverhalten Organischer Grundwasser-Inhaltsstoffe Und Daraus Resultierende Ansätze Zur Beurteilung von Monitored Natural Attenuation (MNA). *TerraTech* **1999**, *5*, 1–14.

(2) Wiedemeier, T. H. *Natural Attenuation of Fuels and Chlorinated Solvents in the Subsurface*; John Wiley & Sons, 1999.

(3) Pecoraino, G.; Scalici, L.; Avellone, G.; Ceraulo, L.; Favara, R.; Candela, E. G.; Provenzano, M. C.; Scaletta, C. Distribution of Volatile Organic Compounds in Sicilian Groundwaters Analysed by Head Space-Solid Phase Micro Extraction Coupled with Gas Chromatography Mass Spectrometry (SPME/GC/MS). *Water Res.* **2008**, *42*, 3563–3577.

(4) McCarty, P. L. Groundwater Contamination by Chlorinated Solvents: History, Remediation Technologies and Strategies. In *In Situ Remediation of Chlorinated Solvent Plumes*; Stroo, H. F., Ward, C. H., Eds.; Springer: New York, NY, USA, 2010; p 1–28.

(5) Tratnyek, P. G.; Johnson, R. L.; Lowry, G. V.; Brown, R. A. In Situ Chemical Reduction for Source Remediation. In *Chlorinated Solvent Source Zone Remediation*; Kueper, B. H., Stroo, H. F., Vogel, C. M., Ward, C. H., Eds.; Springer New York: New York, NY, 2014; p 307–351.

(6) Pennell, K. D.; Cápiro, N. L.; Walker, D. I. Surfactant and Cosolvent Flushing. In *Chlorinated Solvent Source Zone Remediation*; Kueper, B. H., Stroo, H. F., Vogel, C. M., Ward, C. H., Eds.; Springer: New York, NY, USA, 2014; p 353–394.

(7) Kingston, J. L. T.; Johnson, P. C.; Kueper, B. H.; Mumford, K. G. In Situ Thermal Treatment of Chlorinated Solvent Source Zones. In *Chlorinated Solvent Source Zone Remediation*; Kueper, B. H., Stroo, H. F., Vogel, C. M., Ward, C. H., Eds.; Springer: New York, NY, 2014; pp 509–557.

(8) Sweeny, K. H. Treatment of Reducible Halohydrocarbon Containing Aqueous Stream. US Patent No. 4,219,419, 1980.

(9) Gillham, R. W.; O'Hannesin, S. F. Enhanced Degradation of Halogenated Aliphatics by Zero-Valent Iron. *Groundwater* **1994**, *32*, 958–967.

(10) O'Hannesin, S. F.; Gillham, R. W. Long-Term Performance of an In Situ "Iron Wall" for Remediation of VOCs. *Groundwater* **1998**, *36*, 164–170.

(11) Noubactep, C. Investigating the Processes of Contaminant Removal in Fe0/H2O Systems. *Korean J. Chem. Eng.* **2012**, *29*, 1050–1056.

(12) Filip, J.; Zboril, R.; Schneeweiss, O.; Zeman, J.; Cernik, M.; Kvapil, P.; Otyepka, M. Environmental Applications of Chemically Pure Natural Ferrihydrite. *Environ. Sci. Technol.* **2007**, *41*, 4367–4374.

(13) Yan, W.; Lien, H.-L.; Koel, B. E.; Zhang, W. Iron Nanoparticles for Environmental Clean-up: Recent Developments and Future Outlook. *Environ. Sci. Process. Impacts* **2013**, *15*, 63–77.

(14) Mu, Y.; Jia, F.; Ai, Z.; Zhang, L. Iron Oxide Shell Mediated Environmental Remediation Properties of Nano Zero-Valent Iron. *Environ. Sci.: Nano* **2017**, *4*, 27–45.

(15) Wang, C.; Baer, D. R.; Amonette, J. E.; Engelhard, M. H.; Antony, J.; Qiang, Y. Morphology and Electronic Structure of the Oxide Shell on the Surface of Iron Nanoparticles. *J. Am. Chem. Soc.* **2009**, *131*, 8824–8832.

(16) Kumar, N.; Auffan, M.; Gattacceca, J.; Rose, J.; Olivi, L.; Borschneck, D.; Kvapil, P.; Jublot, M.; Kaifas, D.; Malleret, L.; Doumenq, P.; Bottero, J.-Y. Molecular Insights of Oxidation Process of Iron Nanoparticles: Spectroscopic, Magnetic, and Microscopic Evidence. *Environ. Sci. Technol.* **2014**, *48*, 13888–13894.

(17) O 'Carroll, D.; Sleep, B.; Krol, M.; Boparai, H.; Kocur, C. Nanoscale Zero Valent Iron and Bimetallic Particles for Contaminated Site Remediation. *Adv. Water Resour.* **2013**, *51*, 104–122.

(18) Lien, H.-L.; Zhang, W. Transformation of Chlorinated Methanes by Nanoscale Iron Particles. *J. Environ. Eng.* **1999**, *125*, 1042–1047.

(19) Xu, Y.; Zhang, W. Subcolloidal Fe/Ag Particles for Reductive Dehalogenation of Chlorinated Benzenes. *Ind. Eng. Chem. Res.* **2000**, *39*, 2238–2244.

(20) Colombo, A.; Dragonetti, C.; Magni, M.; Roberto, D. Degradation of Toxic Halogenated Organic Compounds by Iron-Containing Mono-, Bi- and Tri-Metallic Particles in Water. *Inorg. Chim. Acta* **2015**, *431*, 48–60.

(21) Kim, Y. H.; Carraway, E. R. Reductive Dechlorination of TCE by Zero Valent Bimetals. *Environ. Technol.* **2003**, *24*, 69–75.

(22) Cwiertny, D. M.; Bransfield, S. J.; Livi, K. J. T.; Fairbrother, D. H.; Roberts, A. L. Exploring the Influence of Granular Iron Additives on 1,1,1-Trichloroethane Reduction. *Environ. Sci. Technol.* **2006**, *40*, 6837–6843.

(23) Schreier, C. G.; Reinhard, M. Catalytic Hydrodehalogenation of Chlorinated Ethylenes Using Palladium and Hydrogen for the Treatment of Contaminated Water. *Chemosphere* **1995**, *31*, 3475–3487.

(24) Zhang, W.; Wang, C.-B.; Lien, H.-L. Treatment of Chlorinated Organic Contaminants with Nanoscale Bimetallic Particles. *Catal. Today* **1998**, *40*, 387–395.

(25) Lowry, G. V.; Reinhard, M. Hydrodehalogenation of 1- to 3-Carbon Halogenated Organic Compounds in Water Using a Palladium Catalyst and Hydrogen Gas. *Environ. Sci. Technol.* **1999**, *33*, 1905–1910.

(26) Park, K. T.; Klier, K.; Wang, C. B.; Zhang, W. X. Interaction of Tetrachloroethylene with Pd(100) Studied by High-Resolution X-Ray Photoemission Spectroscopy. *J. Phys. Chem. B* **1997**, *101*, 5420–5428.

(27) Sriwatanapongse, W.; Reinhard, M.; Klug, C. A. Reductive Hydrodechlorination of Trichloroethylene by Palladium-on-Alumina Catalyst: 13C Solid-State NMR Study of Surface Reaction Precursors. *Langmuir* **2006**, *22*, 4158−4164.

(28) He, F.; Zhao, D. Hydrodechlorination of Trichloroethene Using Stabilized Fe-Pd Nanoparticles: Reaction Mechanism and Effects of Stabilizers, Catalysts and Reaction Conditions. *Appl. Catal., B* **2008**, *84*, 533−540.

(29) Phenrat, T.; Saleh, N.; Sirk, K.; Tilton, R. D.; Lowry, G. V. Aggregation and Sedimentation of Aqueous Nanoscale Zerovalent Iron Dispersions. *Environ. Sci. Technol.* **2007**, *41*, 284−290.

(30) Kocur, C. M.; O'Carroll, D. M.; Sleep, B. E. Impact of nZVI Stability on Mobility in Porous Media. *J. Contam. Hydrol.* **2013**, *145*, 17−25.

(31) He, F.; Zhao, D. Manipulating the Size and Dispersibility of Zerovalent Iron Nanoparticles by Use of Carboxymethyl Cellulose Stabilizers. *Environ. Sci. Technol.* **2007**, *41*, 6216−6221.

(32) Saleh, N.; Sirk, K.; Liu, Y.; Phenrat, T.; Dufour, B.; Matyjaszewski, K.; Tilton, R. D.; Lowry, G. V. Surface Modifications Enhance Nanoiron Transport and NAPL Targeting in Saturated Porous Media. *Environ. Eng. Sci.* **2007**, *24*, 45−57.

(33) Phenrat, T.; Saleh, N.; Sirk, K.; Kim, H.-J.; Tilton, R. D.; Lowry, G. V. Stabilization of Aqueous Nanoscale Zerovalent Iron Dispersions by Anionic Polyelectrolytes: Adsorbed Anionic Polyelectrolyte Layer Properties and Their Effect on Aggregation and Sedimentation. *J. Nanopart. Res.* **2008**, *10*, 795−814.

(34) Laumann, S.; Micic, V.; Lowry, G. V.; Hofmann, T. Carbonate Minerals in Porous Media Decrease Mobility of Polyacrylic Acid Modified Zero-Valent Iron Nanoparticles Used for Groundwater Remediation. *Environ. Pollut.* **2013**, *179*, 53−60.

(35) He, F.; Zhao, D. Preparation and Characterization of a New Class of Starch-Stabilized Bimetallic Nanoparticles for Degradation of Chlorinated Hydrocarbons in Water. *Environ. Sci. Technol.* **2005**, *39*, 3314−3320.

(36) Zhang, M.; He, F.; Zhao, D.; Hao, X. Degradation of Soil-Sorbed Trichloroethylene by Stabilized Zero Valent Iron Nanoparticles: Effects of Sorption, Surfactants, and Natural Organic Matter. *Water Res.* **2011**, *45*, 2401−2414.

(37) Phenrat, T.; Schoenfelder, D.; Kirschling, T. L.; Tilton, R. D.; Lowry, G. V. Adsorbed Poly(aspartate) Coating Limits the Adverse Effects of Dissolved Groundwater Solutes on Fe0 Nanoparticle Reactivity with Trichloroethylene. *Environ. Sci. Pollut. Res.* **2015**, 1−13.

(38) Tiraferri, A.; Chen, K. L.; Sethi, R.; Elimelech, M. Reduced Aggregation and Sedimentation of Zero-Valent Iron Nanoparticles in the Presence of Guar Gum. *J. Colloid Interface Sci.* **2008**, *324*, 71−79.

(39) Comba, S.; Dalmazzo, D.; Santagata, E.; Sethi, R. Rheological Characterization of Xanthan Suspensions of Nanoscale Iron for Injection in Porous Media. *J. Hazard. Mater.* **2011**, *185*, 598−605.

(40) Xue, D.; Sethi, R. Viscoelastic Gels of Guar and Xanthan Gum Mixtures Provide Long-Term Stabilization of Iron Micro- and Nanoparticles. *J. Nanopart. Res.* **2012**, *14*, 1239.

(41) San Román, I.; Galdames, A.; Alonso, M. L.; Bartolomé, L.; Vilas, J. L.; Alonso, R. M. Effect of Coating on the Environmental Applications of Zero Valent Iron Nanoparticles: The Lindane Case. *Sci. Total Environ.* **2016**, *565*, 795−803.

(42) Kumar, N.; Labille, J.; Bossa, N.; Auffan, M.; Doumenq, P.; Rose, J.; Bottero, J.-Y. Enhanced Transportability of Zero Valent Iron Nanoparticles in Aquifer Sediments: Surface Modifications, Reactivity, and Particle Traveling Distances. *Environ. Sci. Pollut. Res.* **2017**, *24*, 9269−9277.

(43) Vecchia, E. D.; Luna, M.; Sethi, R. Transport in Porous Media of Highly Concentrated Iron Micro- and Nanoparticles in the Presence of Xanthan Gum. *Environ. Sci. Technol.* **2009**, *43*, 8942−8947.

(44) Dong, T.; Luo, H.; Wang, Y.; Hu, B.; Chen, H. Stabilization of Fe−Pd Bimetallic Nanoparticles with Sodium Carboxymethyl Cellulose for Catalytic Reduction of Para-Nitrochlorobenzene in Water. *Desalination* **2011**, *271*, 11−19.

(45) Wang, X.; Le, L.; Alvarez, P. J. J.; Li, F.; Liu, K. Synthesis and Characterization of Green Agents Coated Pd/Fe Bimetallic Nanoparticles. *J. Taiwan Inst. Chem. Eng.* **2015**, *50*, 297−305.

(46) Shi, Z.; Fan, D.; Johnson, R. L.; Tratnyek, P. G.; Nurmi, J. T.; Wu, Y.; Williams, K. H. Methods for Characterizing the Fate and Effects of Nano Zerovalent Iron During Groundwater Remediation. *J. Contam. Hydrol.* **2015**, *181*, 17−35.

(47) Fennell, D. E.; Gossett, J. M.; Zinder, S. H. Comparison of Butyric Acid, Ethanol, Lactic Acid, and Propionic Acid as Hydrogen Donors for the Reductive Dechlorination of Tetrachloroethene. *Environ. Sci. Technol.* **1997**, *31*, 918−926.

(48) Lakaye, F.; De Windt, W.; Mariage, P.-A. Catalytic Composition for Treatment of Soil and Sediment. WO 2011006812 A1, 2010.

(49) Shih, Y.; Hsu, C.; Su, Y. Reduction of Hexachlorobenzene by Nanoscale Zero-Valent Iron: Kinetics, pH Effect, and Degradation Mechanism. *Sep. Purif. Technol.* **2011**, *76*, 268−274.

(50) Wilhelm, S. Galvanic Corrosion Caused by Corrosion Products. In *Galvanic Corrosion*; Hack, H. P., Ed.; American Society for Testing and Materials: Philadelphia, PA, USA, 1988; pp 23−34.

(51) Zhang, X. G. Galvanic Corrosion. In *Uhlig's Corrosion Handbook*, Third ed.; Revie, R. W., Ed.; John Wiley & Sons, Inc.: Hoboken, NJ, USA, 2011; pp 123−143.

(52) He, N.; Li, P.; Zhou, Y.; Ren, W.; Fan, S.; Verkhozina, V. A. Catalytic Dechlorination of Polychlorinated Biphenyls in Soil by Palladium-Iron Bimetallic Catalyst. *J. Hazard. Mater.* **2009**, *164*, 126−132.

(53) Dien, N. T.; De Windt, W.; Buekens, A.; Chang, M. B. Application of Bimetallic Iron (BioCAT Slurry) for Pentachlorophenol Removal from Sandy Soil. *J. Hazard. Mater.* **2013**, *252*, 83−90.

(54) Panias, D.; Taxiarchou, M.; Paspaliaris, I.; Kontopoulos, A. Mechanisms of Dissolution of Iron Oxides in Aqueous Oxalic Acid Solutions. *Hydrometallurgy* **1996**, *42*, 257−265.

(55) Schwertmann, U. Solubility and Dissolution of Iron Oxides. *Plant Soil* **1991**, *130*, 1−25.

(56) Kumar, N.; Omoregie, E. O.; Rose, J.; Masion, A.; Lloyd, J. R.; Diels, L.; Bastiaens, L. Inhibition of Sulfate Reducing Bacteria in Aquifer Sediment by Iron Nanoparticles. *Water Res.* **2014**, *51*, 64−72.

(57) Crane, R. A.; Scott, T. B. Nanoscale Zero-Valent Iron: Future Prospects for an Emerging Water Treatment Technology. *J. Hazard. Mater.* **2012**, *211*, 112−125.

(58) Nešić, S. Key Issues Related to Modelling of Internal Corrosion of Oil and Gas Pipelines − A Review. *Corros. Sci.* **2007**, *49*, 4308−4338.

(59) Zhang, W.-S.; Zhang, Z.-L.; Zhang, X.-W. Effects of Temperature on Hydrogen Absorption into Palladium Hydride Electrodes in the Hydrogen Evolution Reaction. *J. Electroanal. Chem.* **2000**, *481*, 13−23.

(60) Riley, A. M.; Seader, J. D.; Pershing, D. W.; Walling, C. An In-Situ Volumetric Method for Dynamically Measuring the Absorption of Deuterium in Palladium during Electrolysis. *J. Electrochem. Soc.* **1992**, *139*, 1342−1347.

(61) Pilling, M. J.; Seakins, P. W. *Reaction Kinetics*; Oxford University Press: New York, NY, USA, 1995.

(62) Bansal, R. K. *Organic Reaction Mechanisms*, 3rd ed.; Tata McGraw-Hill: New Delhi, India, 2004.

(63) Huang, B.; Qian, W.; Yu, C.; Wang, T.; Zeng, G.; Lei, C. Effective Catalytic Hydrodechlorination of O-, P- and M-Chloronitrobenzene over Ni/Fe Nanoparticles: Effects of Experimental Parameter and Molecule Structure on the Reduction Kinetics and Mechanisms. *Chem. Eng. J.* **2016**, *306*, 607−618.

(64) Zhu, B.-W.; Lim, T.-T. Catalytic Reduction of Chlorobenzenes with Pd/Fe Nanoparticles: Reactive Sites, Catalyst Stability, Particle Aging, and Regeneration. *Environ. Sci. Technol.* **2007**, *41*, 7523−7529.

(65) Yan, W.; Herzing, A. A.; Li, X.; Kiely, C. J.; Zhang, W. Structural Evolution of Pd-Doped Nanoscale Zero-Valent Iron (nZVI) in Aqueous Media and Implications for Particle Aging and Reactivity. *Environ. Sci. Technol.* **2010**, *44*, 4288−4294.

(66) Wang, X.; Zhu, M.; Liu, H.; Ma, J.; Li, F. Modification of Pd−Fe Nanoparticles for Catalytic Dechlorination of 2,4-Dichlorophenol. *Sci. Total Environ.* **2013**, *449*, 157−167.